PNAS
www.pnas.org

Supplementary Information for

Fusogen-mediated neuron-neuron fusion disrupts neural circuit connectivity and alters animal behavior.

Rosina Giordano-Santini, Eva Kaulich, Kate M. Galbraith, Fiona K. Ritchie, Wei Wang, Zhaoyu Li, and Massimo A. Hilliard.

Massimo A. Hilliard
Email: m.hilliard@uq.edu.au

This PDF file includes:

www.pnas.org/cgi/doi/10.1073/pnas.1919063117

Supplementary Information Text

Materials and Methods.

AWC^{ON}-AWC^{OFF} cell-cell fusion. AWC^{ON}-AWC^{OFF} fusion was visualized using the transgene *kyIs405[Pstr-2::DsRed; Psrsx-3::GFP] V*, following expression of *Podr-1::eff-1*, *Podr-1::aff-1*, or concurrent expression of *Pstr-2::eff-1* and *Psrsx-3::eff-1* (see **table S1** for strains). As a control, we expressed a non-fusogenic form of EFF-1 (*Podr-1::eff-1(T173A/N529D)*) [1] as well as the empty plasmid (*Podr-1*). The AWC^{ON} and AWC^{OFF} neurons were considered fused when the red cytoplasmic fluorophore expressed in AWC^{ON} was also present in AWC^{OFF}, and the green cytoplasmic fluorophore expressed in AWC^{OFF} was also present in AWC^{ON}. In a subset of animals, this phenotype was accompanied by fusion with one or two AWB neurons, as evidenced by the presence of the red cytoplasmic fluorophore in these cells. We only quantified the mixing of fluorophores between AWC^{ON} and AWC^{OFF} in the absence of fusion with AWB. For AWC^{ON}-AWC^{OFF} fusion following conditional expression of EFF-1, 1 day-old-adult (DOA) animals expressing *Phsp-16.2::eff-1*, together with their non-transgenic siblings and wild-type controls, were heat-shocked at 30 ºC for 1 h and allowed to recover at 20 ºC [2]. Animals were scored for neuronal fusion 48 h later.

AWC^{ON}-AWB cell-cell fusion and fusion with ASI. AWC^{ON}-AWB fusion was visualized using the transgene *kyIs405[Pstr-2::DsRed; Psrsx-3::GFP] V*, following concurrent expression of *Pstr-1::eff-1* and *Pstr-2::eff-1* (see **table S1** for strains). For quantification experiments, the AWC^{ON} and AWB neurons were considered fused when the red cytoplasmic fluorophore expressed in AWC^{ON} was also present in either one or

both AWB neurons, and the green cytoplasmic fluorophore expressed in AWB was also present in AWC^{ON}. These fusion events were accompanied in some animals by fusion with another pair of chemosensory neurons, identified as ASI left and right using the transgenes *otIs264[Pceh-36::TagRFP] III; kyIs128[Pstr-3::GFP]*. Fusion events quantified in **Fig. 2G** do not include AWC^{ON}-AWB neurons fused with ASI neurons.

AWC^{OFF}-AWB cell-cell fusion. AWC^{OFF}-AWB fusion was visualized using the transgene *kyIs104[Pstr-1::GFP] X*, following expression of *Psrsx-3::eff-1* (see **table S1** for strains). Animals with AWC^{OFF}-AWB fusion were identified by the diffusion of the green cytoplasmic fluorophore from AWB to AWC^{OFF}. AWC^{OFF} was identified based on its location and stereotypical cell body, axon, and cilia morphology.

PLN-PLM cell-cell fusion. Fusion between PLM and PLN neurons was visualized by expressing a red cytoplasmic fluorophore in PLN neurons (*Plad-2::mCherry*), and the *zdIs5[Pmec-4::GFP] I* transgene for expression of green cytoplasmic fluorophore in PLM neurons, following concurrent expression of *Plad-2::eff-1* and *Pmec-4::eff-1* (see **table S1** for strains). The PLN and PLM neurons were considered fused when the red cytoplasmic fluorophore expressed in PLN was also present in PLM, and the green cytoplasmic fluorophore expressed in PLM was also present in PLN.

AWC-AWB-AMsh cell-cell fusion. AWC-AWB-AMsh fusion was visualized using the transgenes *nsIs142[pF16F9.3::DsRed] IV* and *vdEx554/7[Podr-1::gfp]*, following expression of *pF16F9.3::aff-1* and *Podr-1::aff-1*. The AWC and AMsh, and/or AWB

and AMsh neurons and glia were considered fused when the red cytoplasmic fluorophore expressed in AMsh was also present in AWC or AWB, and the green cytoplasmic fluorophore expressed in AWC or AWB was also present in AMsh. Fusion events quantified in **Fig. S4** include fusion between AWC and AMsh, AWB and AMsh, and AWC, AWB and AMsh. This experiment was performed in the dauer constitutive background *daf-7(e1372)*, and both adult and dauer animals were cultured at 15 ºC.

Genetic analysis of the site of fusion between AWC and AWB neurons. To analyze the levels of AWC^{ON}-AWB cell-cell fusion in the absence of cilia or dendrites or in animals with premature axon termination, *kyIs405[Pstr-2::DsRed; Psrsx-3::GFP] V; vdEx1729 [Pstr-1::eff-1; Pstr-2::eff-1]* was crossed into *daf-19(m86) II; daf-12(sa204) X*, *dyf-7(m537) X*, *unc-44(e362) IV*, or *unc-76(e911) V.* For each genetic cross, a wild-type sibling was isolated as a control (see **table S1** for strains). Premature axon termination mutant animals with a two AWC^{OFF} phenotype were excluded from the analysis (68 out of 166 animals for *unc-76*, 1 out of 120 animals for *unc-44*). *unc-44* mutant animals with a two AWC^{ON} phenotype were included in the analysis (28 out of 120 animals). All fusion events between one or two AWB neurons and AWC^{ON} were counted, regardless of the presence or absence of fusion with ASI neurons. For *unc-76* mutant animals and corresponding wild-type control, AWC^{ON}-AWB fusion events were categorized into AWC^{ON} and ipsilateral AWB fusion, AWC^{ON} and contralateral AWB fusion, and AWC^{ON} and both AWB neurons fusion, depending on the presence of the red fluorophore from AWC^{ON} in the ipsilateral, contralateral or both AWB neurons, respectively. To analyze the levels of AWC^{OFF}-AWB cell-cell fusion in the absence of cilia or dendrites or

in animals with premature axon termination, *kyIs104[Pstr-1::GFP] X; vdEx1519[Psrsx-3::eff-1]* was crossed into *daf-19(m86) II*, *dyf-7(m537) X*, or *unc-44(e362) IV*. For each genetic cross, a wild-type sibling was isolated as a control (see **table S1** for strains). The analysis of AWC^{OFF}-AWB fusion was conducted in animals grown on *E. coli* HB101, as we serendipitously found that the rates of fusion were increased in these conditions.

Kaede diffusion analysis of cell-cell fusion. Kaede diffusion experiments were performed using an LSM 710 META confocal microscope, equipped with a Plan-Apochromat 63x/1.4 Oil DIC M27 objective and Zen 2012 SP2 software. L4 animals or young adults were mounted on 3.5% agar pads in 0.05% tetramisole in M9 buffer, positioned to obtain a dorso-ventral view of both AWC neurons. A z-stack including both AWC neurons was obtained before, immediately after, and 30 min after conversion of Kaede in one of the neurons. Green fluorescence was visualized with a 488 nm laser (5% power) and red fluorescence was visualized with a 543 nm laser (2% power); for both channels, the gain was adjusted to prevent saturation. Kaede was converted in only one of the AWC cell bodies with a 405 nm laser (2% power) and 5,000 iterations, in a region of interest defined by a circle of 13 pixels diameter placed in the cytoplasm, outside the nucleus. One or two rounds of conversion were performed until visible Kaede conversion was achieved (this resulted in the conversion of only a portion of the total Kaede present in the targeted neuron). Image analysis was performed using Fiji v1.0. For calculations of the changes in intensity of converted Kaede, a sum projection of the z-stacks was performed, and two regions of interest were drawn using the green

channel (non-converted Kaede), following the boundaries of each cell body. The mean intensity in the red channel (converted Kaede) was successively measured for each cell body before, after and 30 min after conversion. Changes in intensity of converted Kaede were calculated using the mean intensity before conversion (F0) as a baseline. Animals where more than a 10-fold conversion could not be achieved in the targeted neuron were excluded from the analysis.

Analysis of the localization of GPCRs in fused neurons. To study the localization of SRSX-3::mKate2 and STR-2::GFP in fused neurons and controls, 1DOA animals were mounted on 3.5% agar pads containing 25 mM sodium azide, in 25 mM sodium azide in M9 buffer, and a z-stack around the tip of the nose was imaged using a 100x/1.4 NA oil-immersion objective in a spinning-disk confocal system as described in the microscopy section below. For SRSX-3::mKate2, exposure times of 500 ms and 100 ms were used for the red and green channels, respectively. For STR-2::GFP, an exposure time of 200 ms was used for both channels. Images were subsequently deconvolved as described above, and analyzed using Fiji v1.0. Cross-sections of the cilia were obtained using the Orthogonal View tool, and together with each plane of the z-stack, were used to determine the presence or absence of the tagged GPCR in each neuron.

Analysis of the expression of nuclear localized NLS::TagRFP in fused neurons. To study the presence of NLS::TagRFP in fused neurons and controls, 1DOA, 2DOA and 3DOA animals were mounted on 3.5% agar pads in 0.05% tetramisole in M9, and visualized using a Zeiss Axio Imager Z1 microscope. If no red fluorescence could be

observed in the nucleus of a neuron, the NLS::TagRFP marker was considered to be absent in that cell. Images in **Fig. 3** were obtained as described below in the Microscopy section.

Analysis of the expression of RAB-3 in fused neurons. To study the presence of mCherry::RAB-3 in fused neurons and controls, 1DOA animals were mounted on 3.5% agar pads containing 25 mM sodium azide, in 25 mM sodium azide in M9 buffer. A z-stack around the head of the animal was imaged using a 63x/1.4 NA oil-immersion objective on a spinning-disk confocal system as described in the microscopy section below. Exposure times of 200 ms were used for both the red and green channels. Images were subsequently deconvolved as described above, and analyzed using Fiji v1.0. Each plane of the z-stack was examined, and maximum projections were used to determine the presence or absence of the mCherry::RAB-3 in each neuron.

Microscopy. For illustration purposes, 1DOA animals were mounted on 3.5% agar pads containing 25 mM sodium azide, in 25 mM sodium azide in M9 buffer. Animals were imaged using a LSM 710 META confocal microscope, equipped with a Plan-Apochromat 63x/1.4 Oil DIC M27 objective and Zen 2012 SP2 software, or a spinning-disk confocal system (Marianas; Intelligent Imaging Innovations) consisting of an Axio Observer Z1 (Carl Zeiss AG) equipped with a CSU-W1 spinning-disk head (Yokogawa Electric Co.), a sCMOS camera (ORCA-Flash4.0 V2 Hamamatsu Photonics), a 40x/1.2 NA water-immersion objective, a 63x/1.4 NA oil-immersion objective, and a 100x/1.4 NA oil-immersion objective. For the spinning-disk confocal system, image acquisition was

performed using SlideBook 6.0 (Intelligent Imaging Innovations), and sampling distances of xy = 156 nm and z = 160 nm, xy = 99 nm and z = 130 nm, and xy = 63 nm and z = 130 nm, for the 40x, 63x, and 100x objectives, respectively. Green fluorescence was visualized with a 488 nm laser and red fluorescence was visualized with a 543 nm laser. Images were deconvolved with Huygens Professional v18.04 (Scientific Volume Imaging) run on a GPU-accelerated computer (3x NVIDIA® Tesla® V100) using the CMLE algorithm, with a signal to noise ratio of 20, a background of 100, and 40 iterations. Images were analyzed using Fiji v1.0. Cross-sections of the head of the animals were obtained using the Orthogonal View tool. Maximum z-projections were used to visualize all neurons in a 2D image. Brightness and contrast were adjusted to facilitate the visualization of all fluorophores in the neurons of interest. For images obtained using the LSM 710 META confocal microscope, the Smooth tool was applied to all channels to remove random noise.

Behavior. Chemosensory assays on individual animals were performed as previously described [3-5]. First, 6-8 adult animals of all tested strains were transferred to 10 cm diameter plates seeded with *E. coli* HB101. L4 or 1DOA progeny were then mounted on 3.5% agar pads in 0.05% tetramisole in M9 buffer, and screened under the compound microscope for the phenotype of interest. For AWC^{ON}-AWC^{OFF} fusion, animals in which these neurons had also undergone fusion with AWB cells were excluded. Similarly, for AWC^{OFF}-AWB fusion, animals in which these neurons had also undergone fusion with other neurons were excluded. For AWC^{ON}-AWB fusion, only animals in which AWC^{ON} and both AWB neurons had fused were selected, excluding the animals in which ASI

neurons had also fused. Finally, wild-type and transgenic controls were selected based on a wild-type phenotype. Selected animals were recovered on *E. coli* HB101-seeded plates, and tested 24 h and 48 h later. Test plates were prepared 24 h earlier as previously described [3], and allowed to dry with the lid off for 1 h before the assay. For each assay, an individual animal was first transferred to an unseeded nematode growth medium plate using halocarbon oil, and allowed to crawl for ~15-30 min to clean it of bacteria [6]. Two drops of 1 µl of the odorant were placed at one end of the test plate, and two drops of 1 µl of ethanol (control) were placed at the other end. The animal was then immediately placed in the center of the test plate, which was placed on a flat surface with the lid on at room temperature (~22 ºC). An hour later, the animal was removed from the plate and placed on a small HB101-seeded plate. A photo of the test plate was taken to record the traces left by the animal on the agar. Animals were tested once or twice on the same day, and allowed to recover on seeded plates for a minimum of 1 h at 20 ºC between assays. All odorants were obtained from Sigma Aldrich at a purity of > 99%. Molecular grade ethanol was used for dilutions and controls. Dilutions of odorants were prepared freshly and were as follows: benzaldehyde 1:200, butanone 1:1,000, pentanedione 1:10,000, and nonanone 1:10. For discrimination assays, butanone was added to the medium before pouring the test plates, as previously described [5]. For analysis, individual photos of the test plates were analyzed using Adobe Illustrator CC 22.1, where a mask in the shape of a square divided in six horizontal regions was fitted to the plate boundaries. Using these regions, the traces left by the animal were given a score between -6 (representing repulsion) and 6 (representing attraction) as previously described [3]. Individual test plates on which the animal had crawled to the side of the plate, had burrowed in the agar, or

could not be recovered after the assay were not included in the analysis. At the end of all assays, all animals were mounted for microscopy and the phenotype was double-checked under a compound microscope. If the phenotype of an animal differed from the original one, all the assays performed with that individual were discarded from the analysis. Some animals from the strains carrying the extrachromosomal array *vdEx1729[Pstr-1::eff-1; Pstr-2::eff-1]* (see **table S1**) have axonal defects such as gaps or shorter axons; these animals have been excluded from behavior experiments. Finally, if the wild-type control group did not respond to the odorant as expected (a median ≤ 2.5 for attraction assays, and ≥ -2.5 for repulsion assays), the assays run in parallel with that control group were discarded. Following this criterion, we discarded 2 out of 59 sets of assays for attraction, and 2 out of 20 sets of assays for repulsion.

Calcium imaging. Animals were grown and selected for the phenotype of interest 24 h before the experiment, as described for behavioral assays, except that selection was performed only at the L4 larval stage. For visualization of calcium responses, individual worms were immobilized by trapping in a micro-channel of a homemade microfluidic chip [7]. The flows of buffer or 10^{-7} pentanedione were delivered using a programmable automatic drug-feeding apparatus (MPS-2, InBio Life Science Instrument Co. Ltd). Fluorescence images were captured using a Prime 95B sCMOS camera. The acquisition was done for one focal plane only. Each animal was imaged twice with 1 min interval to acquire signals from neurons on the left and right sides, with the first imaging position being randomly selected. The average fluorescence intensity of the region of interest (i.e. cell soma) was captured and analyzed using Fiji. The average fluorescence intensity

within the initial 5 s before stimulation was taken as the basal signal F_0. The percentage change of fluorescence intensity relative to the initial intensity F_0, $\Delta F = (F - F_0) / F_0 \times 100$ %, was plotted as a function of time for all curves.

Statistical analysis. Statistical analyses were performed using Microsoft Excel or Prism. Proportions and standard errors of proportions were calculated using the Wald method. For comparison between two independent proportions, the Wald method was used unless conditions for using this method were not satisfied, in which case the Agresti-Coull method was preferred. For Kaede experiments, the changes in intensity ratios between the three time points were compared using a one-way ANOVA. This test was also used to compare the results obtained from calcium imaging analysis. Results from chemosensory assays were analyzed using the Kruskal-Wallis multiple comparison test. In some cases, the wild-type control group was larger than the other groups. To account for these unequal sample sizes, the results of the wild-type control group were randomized using Random.org (https://www.random.org), after which only the first portion of the results with the same sample size as the other groups was used for statistical comparison and representation.

Supplementary Figure 1

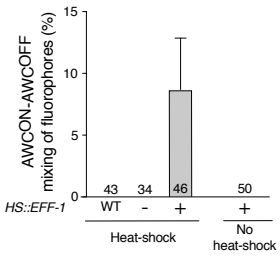

Fig. S1. Mixing of fluorophores between AWC^{ON} and AWC^{OFF} neurons occurs following expression of EFF-1 by a heat-shock promoter. Quantification of AWC^{ON}-AWC^{OFF} mixing of fluorophores in wild-type (WT) animals, and *HS::EFF-1* transgenic animals (+) and their non-transgenic siblings (-), following heat-shock treatment. Quantification of this phenotype in *HS::EFF-1* transgenic animals (+) in the absence of heat-shock treatment is also shown. Mixing of fluorophores between AWC^{ON} and AWC^{OFF} only occurs following the expression of EFF-1. The proportions and SE were calculated using the Wald method for proportions.

Supplementary Figure 2

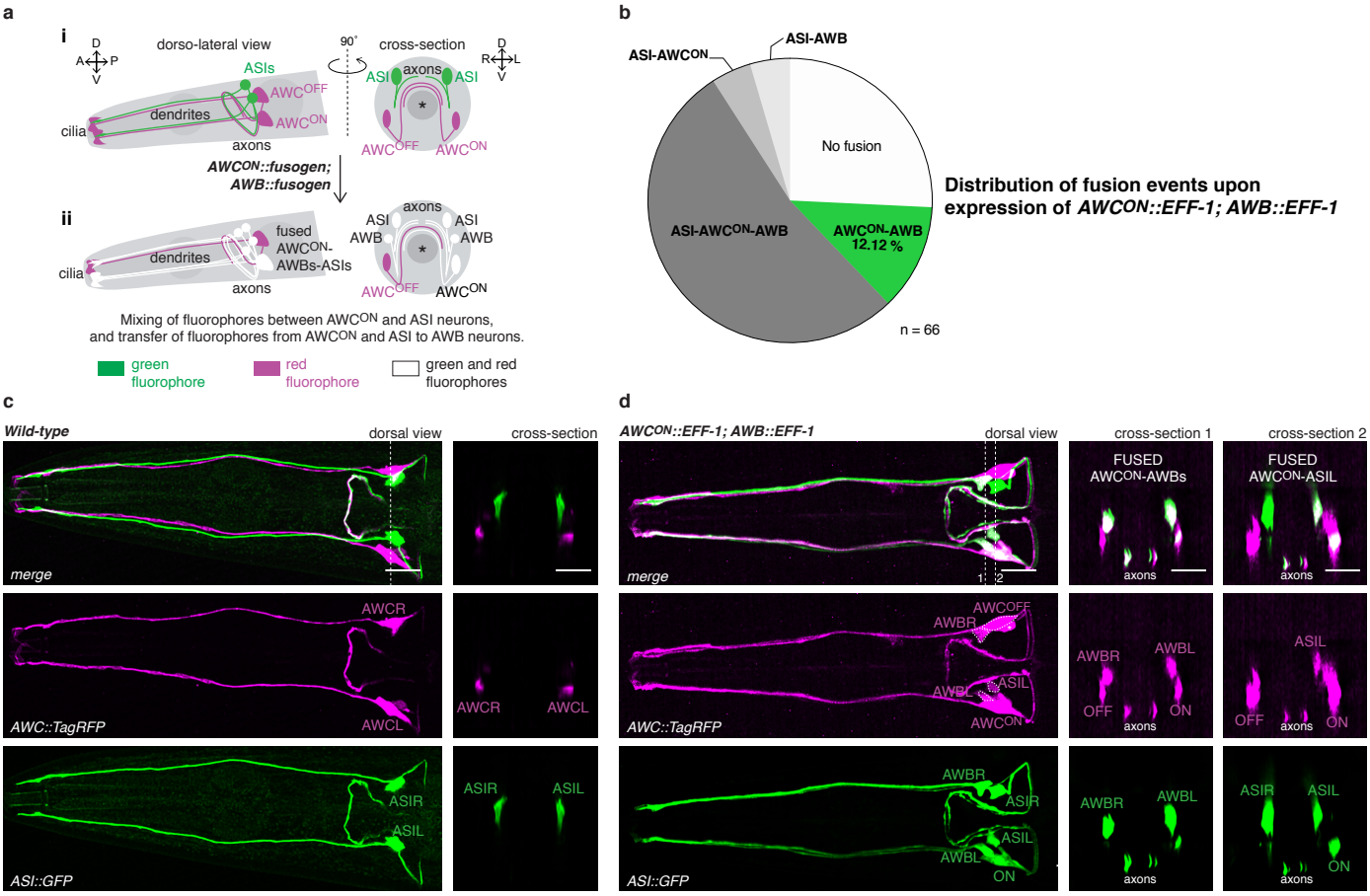

Fig. S2. Neuronal cell-cell fusion between AWC^{ON}, AWB, and ASI neurons. (a) Schematic representation of the AWC, AWB and ASI chemosensory neurons and the fusion assay used to determine the identity of the chemosensory neurons fused with AWC^{ON} and AWB. **i** In a wild-type animal, AWC neurons express a cytoplasmic red fluorophore (*Pceh-36::TagRFP*), whereas the ASI neurons express a cytoplasmic green fluorophore (*Pstr-3::GFP*). **ii** Expression of fusogens in the AWC^{ON} neuron and the AWB neurons (*AWC^{ON}::fusogen; AWB::fusogen*) results in the diffusion of both fluorophores from AWC^{ON} and ASI to AWB neurons, and in mixing of red and green fluorophores between AWC^{ON} and ASI. Asterisk represents the pharynx. A: anterior, P: posterior, D: dorsal, V: ventral, L: left and R: right. **(b)** Quantification and distribution of all fusion events between AWC^{ON}, AWB, and ASI neurons in 1-day-old adult animals expressing *AWC^{ON}::fusogen; AWB::fusogen*. N values are indicated in the graph. Note that in this strain, AWC^{ON} and ASI also undergo cell-cell fusion without necessarily fusing with AWB. **(c, d)** Representative confocal maximum z-projection images of the head of a wild-type animal **(c)**, and an animal with AWC^{ON}, AWB and ASI left fusion **(d)**. Cross-sections at the level of the cell bodies are shown on the right of each panel, and indicated by dotted lines on the dorsal views. Scale bars: 10 µm.

Supplementary Figure 3

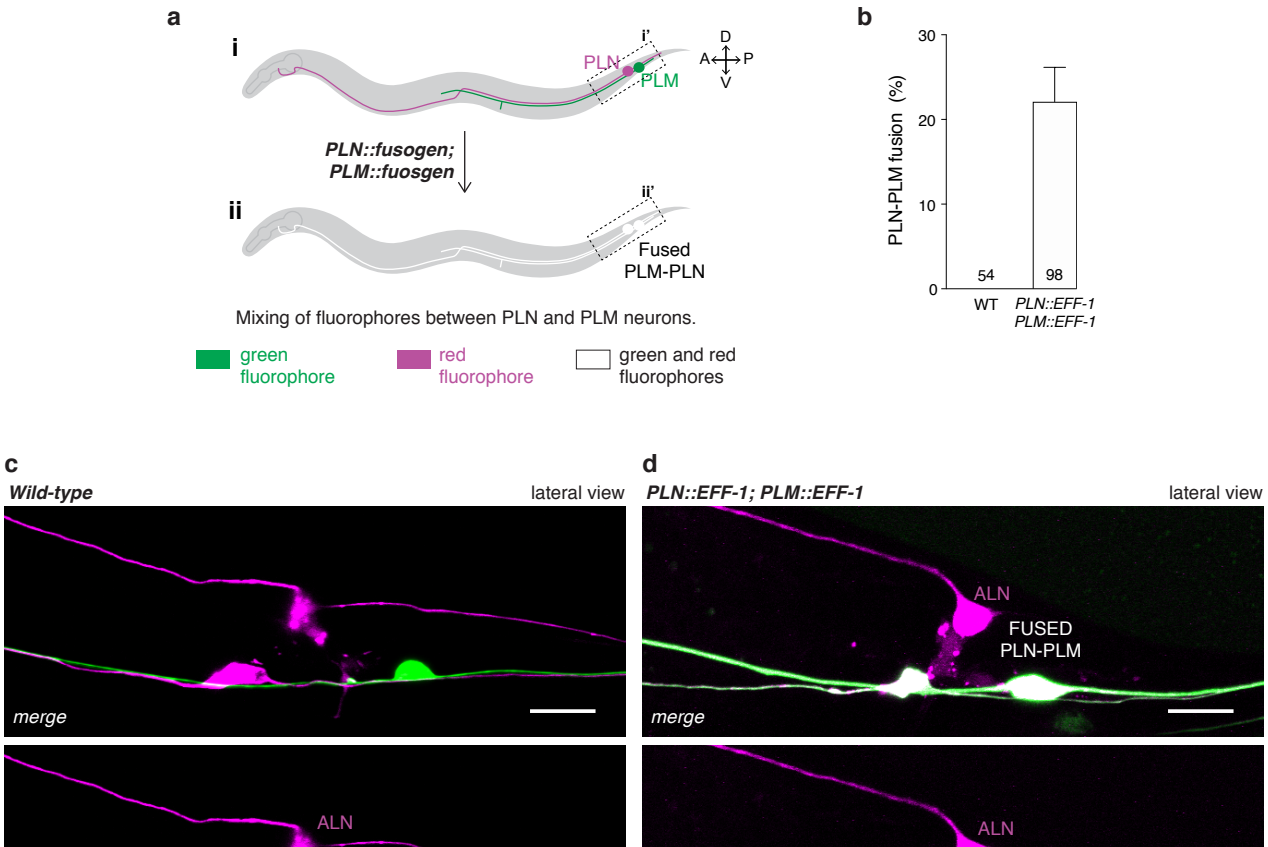

Fig. S3. Neuronal cell-cell fusion between the oxygen-sensing PLN neuron and the mechanosensory PLM neuron. (a) Schematic representation of the PLN and PLM neurons and the fusion assay used in this study. **i** In a wild-type animal, the PLN neuron expresses a cytoplasmic red fluorophore (*Plad-2::mCherry*), whereas the PLM neuron expresses a cytoplasmic green fluorophore (*Pmec-4::GFP*). **ii** Expression of fusogens in the two neurons (*PLN::fusogen; PLM::fusogen*) results in the mixing of red and green fluorophores between PLN and PLM. Only the neurons on the left side of the animal are represented. A: anterior, P: posterior, D: dorsal, V: ventral. **(i')** and **(ii')** highlight the regions shown in **(c)** and **(d)**, respectively. **(b)** Quantification of PLN-PLM fusion events in 1-day-old adult animals expressing *PLN::EFF-1; PLM::EFF-1* (*Plad-2::eff-1; Pmec-4::eff-1*). WT: wild-type. N values are indicated in the graph. **(c, d)** Representative confocal maximum z-projection images of a wild-type animal **(c)**, and an animal with fused PLN-PLM neurons **(d)**. Note that the ALN neuron in the dorsal part of the animal also expresses the cytoplasmic red fluorophore. Scale bars: 10 μm.

Supplementary Figure 4

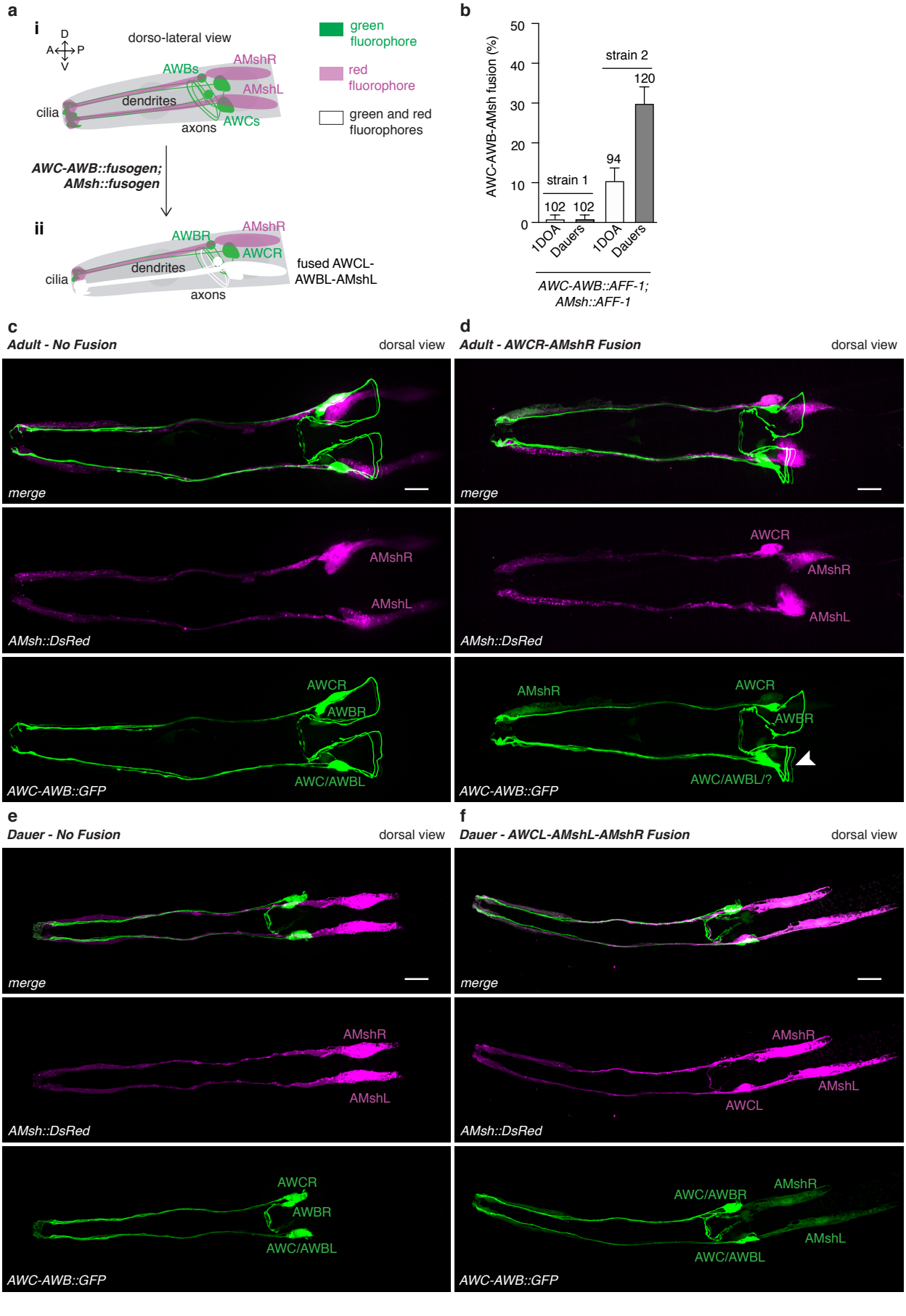

Fig. S4. Neurons-glia fusion in adult and dauer animals. (a) Schematic representation of the AWC and AWB chemosensory neurons and the Amphid sheath (AMsh) glia, and the fusion assay used in this experiment. **i** In a wild-type animal, the AMsh glia express a cytoplasmic red fluorophore (*PF16F9.3::DsRed*), whereas the AWC and AWB neurons express a cytoplasmic green fluorophore (*Podr-1::GFP*). **ii** Expression of fusogens in all cells (*AWC-AWB::fusogen; AMsh::fusogen*) results in the mixing of red and green fluorophores between neurons and glia. Only fusion between the neurons and glia on the left side of the animal is represented. A: anterior, P: posterior, D: dorsal, V: ventral. **(b)** Quantification of neuron-glia fusion events in 1-day-old (1DOA) adult animals (white bars) and dauer animals (gray bars) expressing *AWC-AWB::AFF-1; AMsh::AFF-1* (*Podr-1::aff-1; PF16F9.3::aff-1*). Note that all fusion events where at least one neuron and one glial cell fused are included. Two independent transgenic strains are shown. N values are indicated in the graph. **(c, d)** Representative confocal maximum z-projection images of an adult animal with no fusion **(c)**, and an adult animal with fused AWCR-AMshR **(d)**. A filled arrowhead points to a third axon from another chemosensory neuron fused with one of the AWC or AWB cells. **(e, f)** Representative confocal maximum z-projection images of a dauer animal with no fusion **(e)**, and a dauer animal with fused AWCL-AMshL-AMshR **(f)**. Scale bars: 10 μm.

Supplementary Figure 5

a

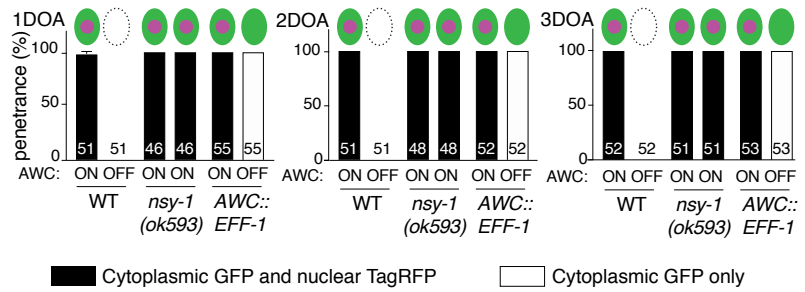

b

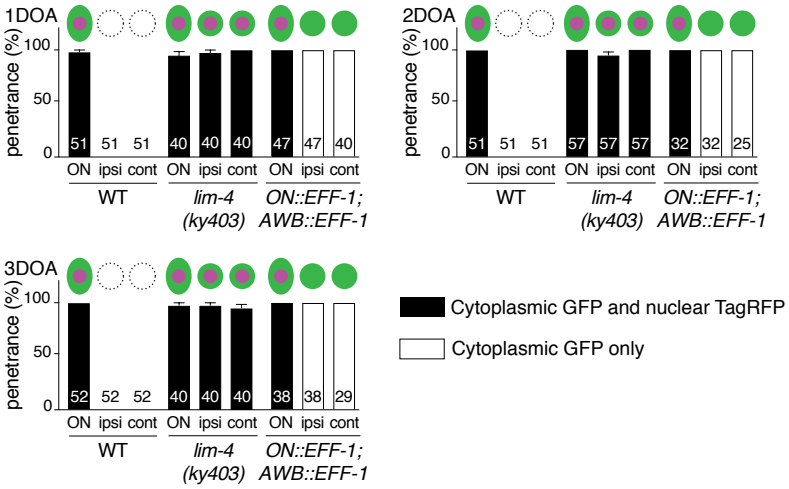

Fig. S5. Fused neurons retain the expression of neuronal cell fate markers.

(a) Quantification of the presence or absence of GFP and nuclear TagRFP in 1-day-old adults (1DOA), 2-day-old adults (2DOA), and 3-day-old adults (3DOA), in wild-type (WT), *nsy-1*, and AWC^{ON}-AWC^{OFF} fused animals (*AWC::EFF-1*). **(b)** Quantification of the presence or absence of GFP and nuclear TagRFP in AWC^{ON} (ON), its ipsilateral AWB (ipsi) and its contralateral AWB (cont), in 1, 2 and 3DOA in wild-type (WT), *lim-4*, and AWC^{ON}-AWB fused animals (*ON::EFF-1; AWB::EFF-1*). Proportions and standard errors were calculated using the Wald method for proportions.

Supplementary Figure 6

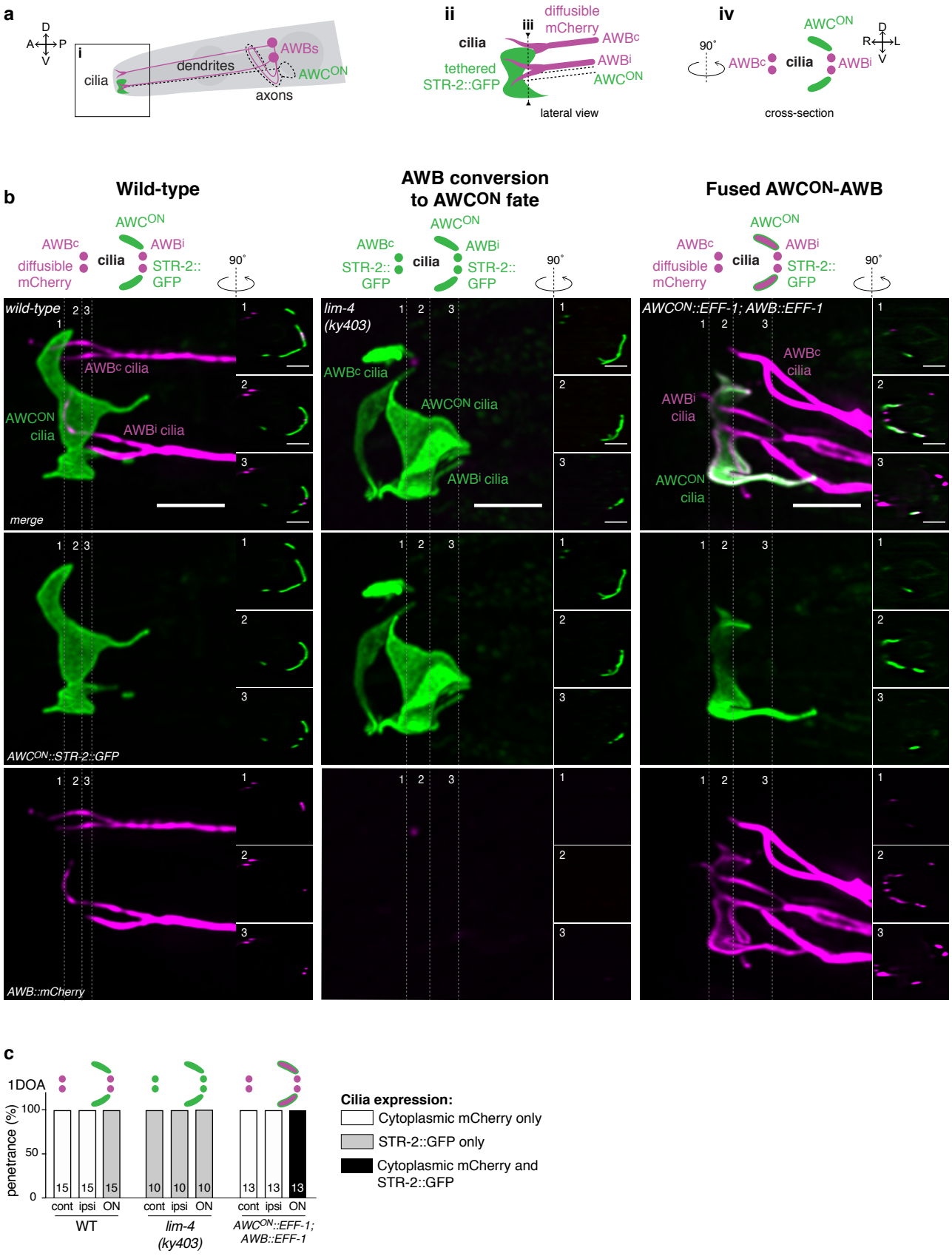

Fig. S6. Cell-cell fusion between AWC^{ON} and AWB does not alter the expression and localization of the GPCR STR-2. (a) Schematic of the fluorescent markers used to assess a change in neuronal expression and localization of the GPCR STR-2 following fusion between the AWC^{ON} and AWB neurons. In the AWC^{ON} neuron, STR-2 tagged with a green fluorophore (STR-2::GFP) is expressed and localized at the cilium, whereas the AWB neurons express a cytoplasmic red fluorophore (diffusible mCherry). **i** shows the region of the chemosensory neurons' cilia, which is depicted in **ii**. **iii** shows the position of the cross-section represented in **iv**. **(b)** In the top row there are representative schemes of each phenotype. Left: in a wild-type animal, STR-2::GFP is present selectively in the cilia of AWC^{ON}, whereas mCherry is expressed in both AWB cilia; middle: in *lim-4* mutant animals, in which AWB cell fate is converted into an AWC^{ON} fate, STR-2::GFP is present in both AWB and the AWC^{ON} neurons; right: in animals with fused AWC^{ON}-AWB neurons, as evidenced by the diffusion of mCherry to AWC^{ON}, STR-2::GFP is only present in the AWC^{ON} cilium, indicating that the fused AWB neurons do not express the AWC^{ON}-specific STR-2 receptor. Second to fourth rows: representative confocal maximum z-projection images of the cilia of AWC^{ON} and AWB neurons in wild-type animals (left), *lim-4* mutant animals (middle), and animals with fused AWC^{ON}-AWB neurons (right). For each animal, cross-sections of the cilia are shown for three different positions, all indicated by vertical dotted lines (1-3) on the lateral views. Scale bars: 5 μm. Note that the cilia of AWB neurons in *lim-4* mutant animals acquire an AWC cilia-like morphology. **(c)** Quantification of the presence or absence of mCherry and STR-2::GFP in the cilium of AWC^{ON} (ON), its ipsilateral AWB neuron (ipsi), and its contralateral AWB neuron (cont) in 1-day-old adults, in wild-type

(WT), *lim-4* mutant animals, and AWC^{ON}-AWB fused animals (*AWC^{ON}::EFF-1; AWB::EFF-1*). N values are indicated in the graph.

Supplementary Figure 7

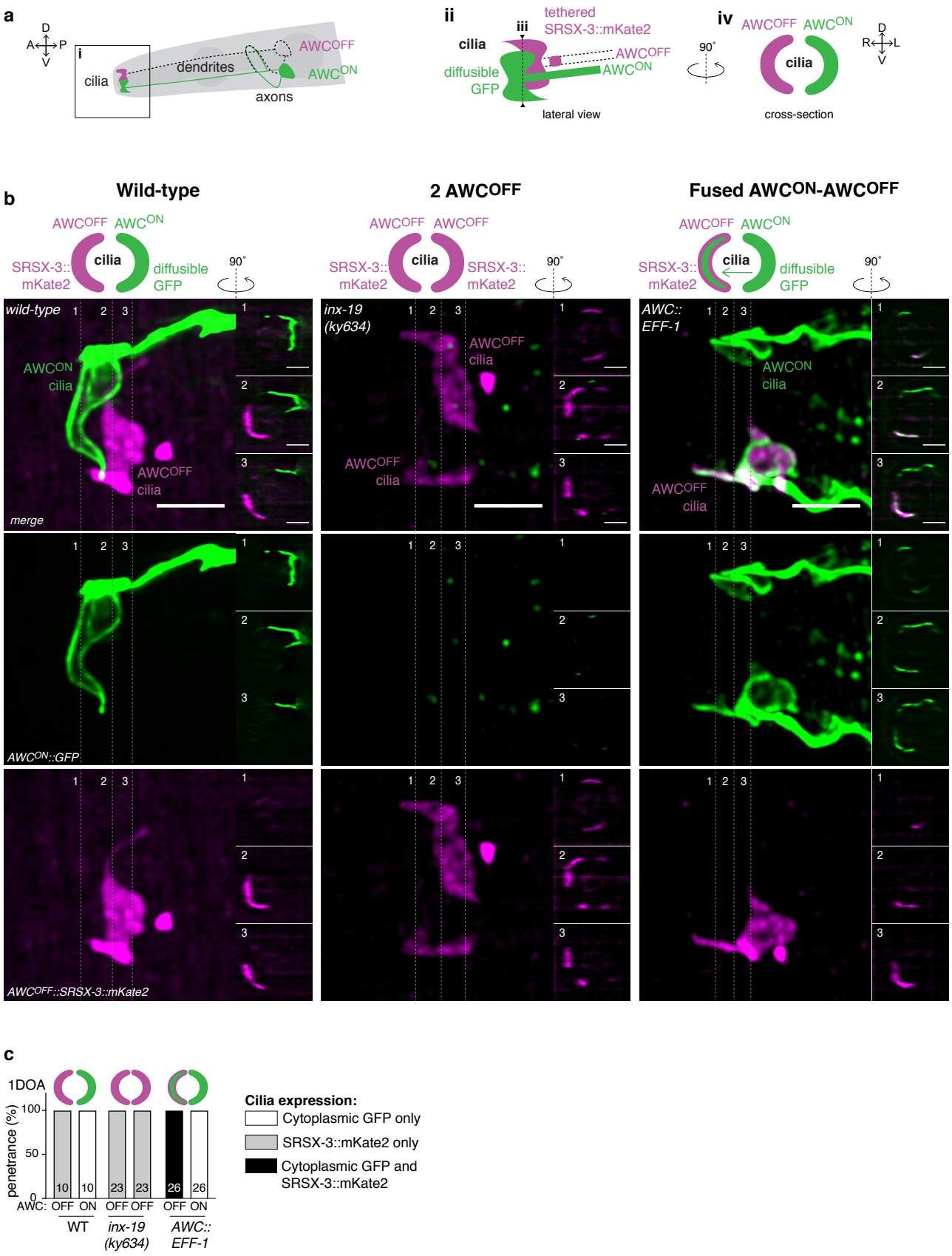

Fig. S7. Cell-cell fusion between AWC^{ON} and AWC^{OFF} does not alter the expression and localization of the GPCR SRSX-3. (a) Schematic of the fluorescent markers used to assess a change in neuronal expression and localization of the SRSX-3 GPCR following fusion of AWC^{ON} and AWC^{OFF} neurons. The AWC^{ON} neuron expresses a cytoplasmic green fluorophore (diffusible GFP), whereas the AWC^{OFF} neuron expresses SRSX-3 tagged with a red fluorophore (SRSX-3::mKate2) which localizes at the cilium. **i** shows the region of the chemosensory neurons' cilia, which is depicted in **ii**. **iii** shows the position of the orthogonal plane represented in **iv**. **(b)** Top row are representative schemes of each phenotype. Left: in a wild-type animal, SRSX-3::mKate2 is expressed and localized in the cilium of AWC^{OFF}, whereas GFP is expressed in AWC^{ON}; middle: in *inx-19* mutant animals, in which both AWC neurons adopt an OFF fate, SRSX-3::mKate2 is expressed in the cilia of both AWC^{OFF} neurons; right: in animals with fused AWC^{ON}-AWC^{OFF} neurons, as evidenced by the diffusion of GFP to AWC^{OFF}, SRSX-3::mKate2 is only localized to the AWC^{OFF} cilium, suggesting that the fused AWC^{ON} neuron does not express the AWC^{OFF}-specific SRSX-3 receptor. Second to fourth rows: representative confocal maximum z-projection images of the cilia of AWC neurons in wild-type animals (left), *inx-19* mutant animals (middle), and animals with fused AWC^{ON}-AWC^{OFF} neurons (right). For each animal, cross-sections of the cilia are shown for three different positions, all indicated by vertical dotted lines (1-3) on the lateral views. Scale bars: 5 μm. **(c)** Quantification of the presence or absence of GFP and SRSX-3::mKate2 in the cilia of AWC neurons in 1-day-old adults, in wild-type (WT) animals, *inx-19* mutant animals, and AWC^{ON}-AWC^{OFF} fused animals (*AWC::EFF-1*). N values are indicated in the graph.

Supplementary Figure 8

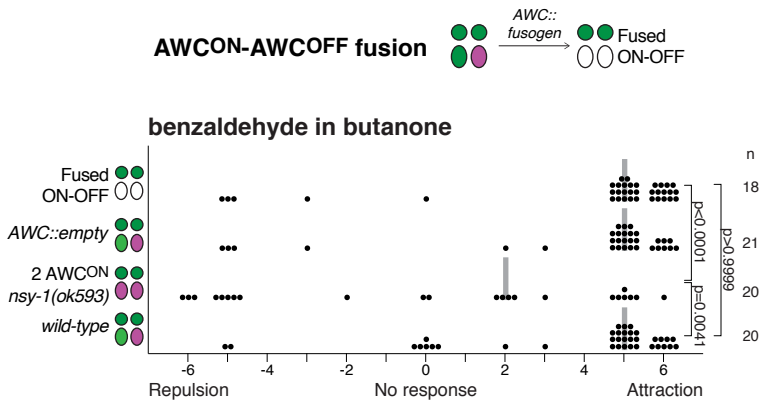

Fig. S8. Animals with fused AWC^{ON}-AWC^{OFF} neurons discriminate between butanone and benzaldehyde. Animals with fused AWC^{ON}-AWC^{OFF} neurons are attracted to benzaldehyde in a saturating field of butanone to the same level as transgenic and wild-type controls, whereas animals with two AWC^{ON} neurons (*nsy-1*) are not able to discriminate between these odorants. Negative values represent repulsion, and positive values represent attraction to the odorant. Data shown are from a minimum of two independent behavioral experiments performed on different days. Each dot represents the result of an individual assay, a vertical gray bar represents the median, and n represents the total number of animals tested for each group. Comparisons between groups were obtained using the Kruskal-Wallis test.

Supplementary Figure 9

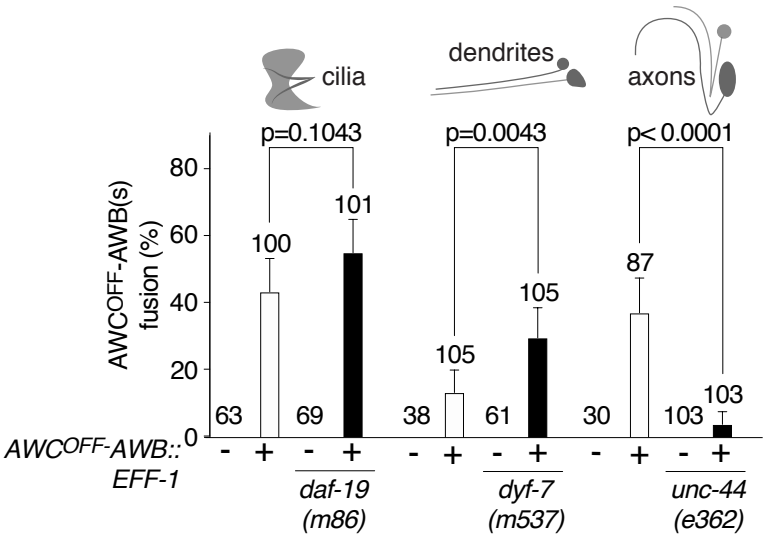

Fig. S9. AWC^{OFF} and AWB neurons fuse at the level of the axon. Quantification of the AWC^{OFF}-AWB fusion events in mutant animals lacking cilia (*daf-19(m86)*), or dendrites (*dyf-7(m537)*), or in animals with premature axon termination (*unc-44(e362)*), and their respective wild-type controls (white bars). The penetrance of fusion events is highly reduced in the absence of full-length axons. Comparisons between groups were obtained using the Wald method for comparing proportions.

Supplementary Figure 10

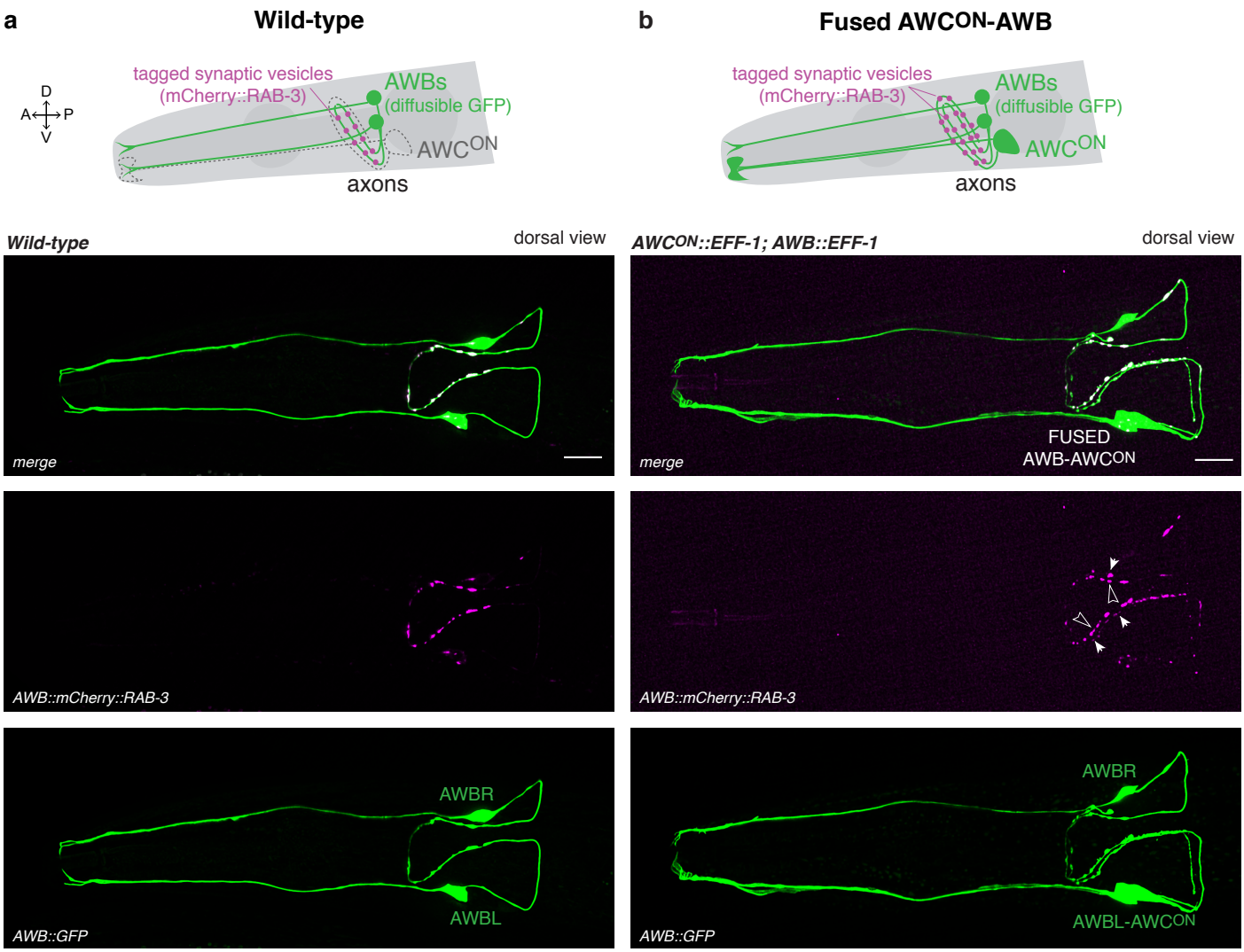

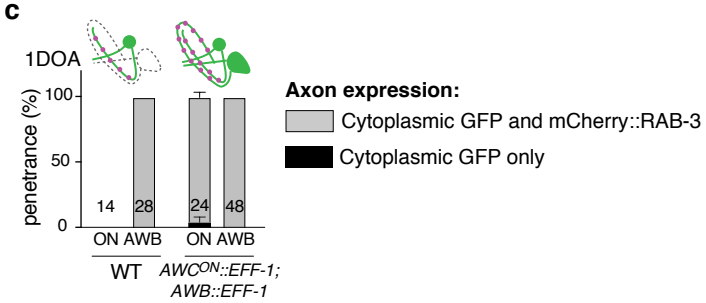

Fig. S10. The synaptic vesicle marker RAB-3 diffuses or is transported between the axons of fused AWC^{ON}-AWB neurons. (a) Top row: schematic of the AWB neurons expressing a cytoplasmic green fluorophore (diffusible GFP) and a synaptic vesicle marker tagged with mCherry (mCherry::RAB-3) in a wild-type animal. Second to fourth rows: representative confocal maximum z-projection image of the head of a wild-type animal. mCherry::RAB-3 is only visible in the axons and soma of the AWB neurons. Scale bars: 10 µm. **(b)** Top row: schematic of an animal with fused AWC^{ON}-AWB neurons, as evidenced by the diffusion of GFP from AWB to AWC^{ON}. Synaptic vesicles (mCherry::RAB-3) are also visible in the AWC^{ON} axon. Second to fourth rows: representative confocal maximum z-projection image of the head of an animal with AWC^{ON}-AWB fusion. Arrowheads show mCherry::RAB-3 in the AWB axons, and filled arrowheads show mCherry::RAB-3 in the AWC^{ON} axon. Scale bars: 10 µm. **(c)** Quantification of the presence of diffusible GFP and mCherry::RAB-3 in 1-day-old adults (1DOA), in wild-type (WT), and in AWC^{ON}-AWB fused animals (*AWC^{ON}::EFF-1; AWB::EFF-1*). ON: AWC^{ON}. Proportions and standard errors were calculated using the Wald method for proportions.

Supplementary Table 1. List of strains used in this study.

STRAIN NAME	GENOTYPE	SOURCE	USE	FIGURE
CX7893	*kyIs405[Pstr-2::DsRed, Psrsx-3::GFP; Pelt-2::GFP] V*	[8]	Wild-type control for AWC^{ON}-AWC^{OFF} fusion, and AWC^{ON}- AWB fusion.	Fig. 1, 2 and 4, Fig, S1, and S8
QH6440	*kyIs405 V; vdEx1494[Podr-1::(empty) 5 ng/µl; Punc-122::RFP]*	This study	Promoter-only control for AWC^{ON}-AWC^{OFF} fusion.	Fig. 1 and 4, Fig. S8
QH6324	*kyIs405 V; vdEx1480[Podr-1::aff-1 5 ng/µl; Punc-122::RFP]*	This study	AFF-1 mediated AWC^{ON}-AWC^{OFF} fusion.	Fig. 1
QH6600	*kyIs405 V; vdEx1575[Podr-1::eff-1 2.5 ng/µl; Punc-122::RFP]*	This study	AWC^{ON}-AWC^{OFF} fusion.	Fig. 1 and 4, Fig. S8
QH6061	*kyIs405 V; hyEx21[Phsp-16.2::eff-1; rol-6(su1006)]*	This study (*hyEx21* [2])	AWC^{ON}-AWC^{OFF} fusion following heat-shock.	Fig. S1
QH6872	*kyIs405 V; vdEx1735[Pstr-2::eff-1 5 ng/µl; Plin-44::mRFP]*	This study	Expression of EFF-1 in AWC^{ON} only.	Fig. 1
QH6487	*kyIs405 V; vdEx1521[Psrsx-3::eff-1 5 ng/µl; Punc-122::RFP]*	This study	Expression of EFF-1 in AWC^{OFF} only.	Fig. 1
QH7069	*kyIs405 V; vdEx1735; vdEx1519[Psrsx-3::eff-1 5 ng/µl; Punc-122::RFP]*	This study	Concurrent expression of EFF-1 in AWC^{ON} and AWC^{OFF}. AWC^{ON}-AWC^{OFF} fusion.	Fig. 1
QH8162	*kyIs405 V; vdEx2348[Podr-1::eff-1(T173A/N529D) 5ng/µl; Punc-122::RFP]*	This study	Non-fusogenic EFF-1 control.	Fig. 1
QH6868	*kyIs405 V; vdEx1731[Pstr-1::(empty) 5 ng/µl; Pstr-2::(empty) 5 ng/µl; Punc-122::RFP]*	This study	Promoter-only control for AWC^{ON}-AWB fusion.	Fig. 2 and 4
QH6866	*kyIs405 V; vdEx1729[Pstr-1::eff-1 5 ng/µl; Pstr-2::eff-1 5 ng/µl; Punc-122::RFP]*	This study	AWC^{ON}-AWB fusion.	Fig. 2 and 4
QH7627	*otIs264[Pceh-36::TagRFP] III; kyIs128[Pstr-3::GFP; lin-15(+)]; vdEx1729*	This study (*otIs264* [9]; *kyIs128* [10])	AWC^{ON}-AWB-ASI fusion.	Fig. S2
CX3553	*lin-15(n765), kyIs104[Pstr-1::GFP; lin-15(+)] X*	[3]	Wild-type control for AWC^{OFF}-AWB fusion.	Fig. 2 and 4
QH6842	*lin-15(n765), kyIs104 X; vdEx1519*	This study	AWC^{OFF}-AWB fusion.	Fig. 2 and 4
QH6875	*lin-15(n765), kyIs104 X; vdEx1738[Psrsx-3::(empty) 5 ng/µl; Punc-122::RFP]*	This study	Promoter-only control for AWC^{OFF}-AWB fusion.	Fig. 2 and 4
QH6599	*vdEx477[Podr-1::eff-1 20 ng/µl; rol-6(su1006)]; vdEx493[Pstr-2::Kaede 50 ng/µl; Punc-122::GFP]*	This study	AWC^{ON}::Kaede; AWC^{ON}-AWC^{OFF} fusion.	Fig. 1
QH6576	*nsy-1(ok593) II; vdEx493*	This study	AWC^{ON}::Kaede; 2 AWC^{ON}.	Fig. 1
QH7397	*kyIs405 V; daf-12(sa204) X; vdEx1729*	This study	AWC^{ON}-AWB fusion control for strain QH7358.	Fig. 5

QH7358	*daf-19(m86) II; kyIs405 V; daf-12(sa204) X; vdEx1729*	This study	AWC^{ON}-AWB fusion in the absence of cilia.	Fig. 5
QH7333	*kyIs405 V; vdEx1729*	This study	AWC^{ON}-AWB fusion control for strain QH7283.	Fig. 5
QH7283	*kyIs405 V; dyf-7(m537) X; vdEx1729*	This study	AWC^{ON}-AWB fusion in the absence of dendrites.	Fig. 5
QH7458	*kyIs405 V; vdEx1729*	This study	AWC^{ON}-AWB fusion control for strain QH7434.	Fig. 5
QH7434	*unc-44(e362) IV; kyIs405 V; vdEx1729*	This study	AWC^{ON}-AWB fusion in premature axon termination animals.	Fig. 5
QH7464	*kyIs405 V; vdEx1729*	This study	AWC^{ON}-AWB fusion control for strain QH7465.	Fig. 5
QH7465	*unc-76(e911), kyIs405 V; vdEx1729*	This study	AWC^{ON}-AWB fusion in premature axon termination animals.	Fig. 5
QH4408	*daf-7(e1372) III; nsIs142[pF16F9.3:DsRed; lin-15(+)] IV; vdEx554[pF16F9.3::aff-1 5 ng/µl; Podr-1::aff-1 5 ng/µl; Podr-1::GFP]*	This study (*nsIs142*[11])	AWC-AWB-AMsh fusion.	Fig. S4
QH4411	*daf-7(e1372) III; nsIs142 IV; vdEx557[pF16F9.3::aff-1 5 ng/µl; Podr-1::aff-1 5 ng/µl; Podr-1::GFP]*	This study	AWC-AWB-AMsh fusion.	Fig. S4
QH7429	*lin-15(n765), kyIs104 X; vdEx1519*	This study	AWC^{OFF}-AWB fusion control for strain QH7456.	Fig. S9
QH7456	*daf-19(m86) II; lin-15(n765); kyIs104 X; vdEx1519*	This study	AWC^{OFF}-AWB fusion in the absence of cilia.	Fig. S9
QH7432	*lin-15(n765), kyIs104 X; vdEx1519*	This study	AWC^{OFF}-AWB fusion control for strain QH7431.	Fig. S9
QH7431	*dyf-7(m537), kyIs104 X; vdEx1519*	This study	AWC^{OFF}-AWB fusion in the absence of dendrites.	Fig. S9
QH7436	*lin-15(n765), kyIs104 X; vdEx1519*	This study	AWC^{OFF}-AWB fusion control for strain QH7435.	Fig. S9
QH7435	*unc-44(e362) IV; lin-15(n765), kyIs104 X; vdEx1519*	This study	AWC^{OFF}-AWB fusion in premature axon termination animals.	Fig. S9
QH7240	*kyIs140[Pstr-2::GFP; lin-15(+)] I; vyIs51[Pstr-2::2xnlsTagRFP; Pofm-1::DsRed] V; vdEx477*	This study (*vyIs51* [12])	AWC^{ON}-AWC^{OFF} fusion. Reprogramming of AWC^{ON}-AWC^{OFF} (nucleus).	Fig. 3 and S5
QH7340	*kyIs140 I; vyIs51 V*	This study	Wild-type control for reprogramming of AWC^{ON}-AWC^{OFF} (nucleus).	Fig. 3 and S5
QH7405	*kyIs140 I; nsy-1(ok593) II; vyIs51 V*	This study	2 AWC^{ON} control for reprogramming of AWC^{ON}-AWC^{OFF} (nucleus).	Fig. 3 and S5
QH7354	*kyIs140 I; vyIs51 V; vdEx1997[Pstr-1::eff-1 2.5ng/µl; Pstr-2::eff-1 2.5 ng/µl; Plin-44::mRFP]*	This study	AWC^{ON}-AWB fusion. Reprogramming of AWC^{ON}-AWB (nucleus).	Fig. 3 and S5
QH7693	*kyIs140 I; vyIs51 V; lim-4(ky403) X*	This study	AWB acquires AWC^{ON} fate control for reprogramming of AWC^{ON}-AWB (nucleus).	Fig. 3 and S5

QH7752	*oyIs65[Pstr-1::mCherry]; lin-15(n765) X; kyEx176[Pstr-2::str-2::GFP; lin-15(+)]*	This study (*oyIs65* [13]; *kyEx176* [14])	Wild-type control for reprogramming of AWC^{ON}-AWB (STR-2::GFP).	Fig. S6
QH7753	*oyIs65; lim-4(ky403), lin-15(n765) X; kyEx176*	This study	AWB conversion to AWC^{ON} fate control for reprogramming of AWC^{ON}-AWB (STR-2::GFP).	Fig. S6
QH7750	*oyIs65/+; lin-15(n765) X; kyEx176; vdEx1729*	This study	AWC^{ON}-AWB fusion. Reprogramming of AWC^{ON}-AWB (STR-2::GFP).	Fig. S6
QH7335	*kyIs140 I; vdSi13[Psrsx-3::srsx-3::mKate2] II*	This study	Wild-type control for reprogramming of AWC^{ON}-AWC^{OFF} (SRSX-3::mKate2).	Fig. S7
QH7428	*inx-19(ky634) I; vdSi13 II*	This study	2 AWC^{OFF} control for reprogramming of AWC^{ON}-AWC^{OFF} (SRSX-3::mKate2).	Fig. S7
QH7356	*kyIs140 I; vdSi13 II; vdEx477*	This study	AWC^{ON}-AWC^{OFF} fusion. Reprogramming of AWC^{ON}-AWC^{OFF} (SRSX-3::mKate2).	Fig. S7
QH3429	*zdIs5[Pmec-4::GFP; lin-15(+)] I; vdEx167[Plad-2::mCherry; Podr-1::DsRed]*	[15]	Wild-type control for PLN-PLM fusion.	Fig. S3
QH4405	*zdIs5 I; vdEx551[Plad-2::mCherry; Pmec-4::eff-1 5 ng/µl;Plad-2::eff-1 5 ng/µl; Podr-1::GFP]*	This study	PLM-PLN fusion.	Fig. S3
CX8446	*kyEx1423[Pstr-1::GCaMP1.0; Punc-122::GFP]*	[16]	Calcium imaging of AWB controls.	Fig. 6
QH7285	*kyEx1423; vdEx1519*	This study	Calcium imaging of AWC^{OFF}-AWB fusion.	Fig. 6
QH8183	*kyIs104 X; vdEx1729; vdEx2357[Pstr-1::mCherry::rab-3]*	This study	Expression of mCherry::rab-3 in AWB with AWC^{ON}-AWB fusion.	Fig. S10
QH8206	*kyIs104 X; vdEx2357*	This study	Expression of mCherry::rab-3 in AWB control for strain QH8183.	Fig. S10

Supplementary Table 2. List of plasmids and cloning methods used in this study.

PLASMID NAME	GENE OF INTEREST	USE	CLONING	PRIMERS
pRGS6	*Podr-1::aff-1*	AWC^{ON}-AWC^{OFF} fusion.	Obtained by cloning PCR amplified *aff-1* into *Podr-1::DsRed* using Kpn I and Bst XI restriction enzymes.	org352 CGGGGTACCATGCGA CTGTGGCAATGGTC org353 ATGCATCCATGTAGA TGGTTAGTAATCAGA TGAATTCTTC
pRGS8	*Podr-1::eff-1*	AWC^{ON}-AWC^{OFF} fusion.	Obtained by cloning PCR amplified *eff-1* into *Podr-1::DsRed* using Kpn I and Bsa AI restriction enzymes.	org350 CGGGGTACCATGGAA CCGCCGTTTGAGTG org351 GTCCACGTATCAAAT GTACTGGCTACTGC
pRGS47	*Podr-1::(empty)*	*Podr-1* control	Obtained by removing *eff-1* from pRGS8 using Nco I restriction enzyme.	
pKG17	*Podr-1::eff-1(T173A/N529D)*	Expression of non-fusogenic form of EFF-1 in AWC^{ON} and AWC^{OFF}.	Obtained by sequential Quik Change reaction of pRGS8 to mutate T173 and N529 residues.	eff1 T173A F GCACGTTCTTCCCAA ATCAGGCACCAATCG GGTGCAGTGAAG eff1 T173A R CTTCACTGCACCCGA TTGGTGCCTGATTTG GGAAGAACGTGC eff1 N529D F2 GGAACCTGCCCAACT TGTGATCAAATCAAT TTCAATGGAATGATG eff1 N529D R2 CATCATTCCATTGAA ATTGATTTGATCACA AGTTGGGCAGGTTCC
pEK7	*Psrsx-3::eff-1*	AWC^{OFF}-AWB fusion.	Obtained by replacing *Podr-1* with *Psrsx-3* (from pRGS7 *Psrsx-3::Kaede*) in pRGS8 using Pvu II and Kpn I restriction enzymes.	
pRGS50	*Psrsx-3::(empty)*	*Psrsx-3* control.	Obtained by removing EFF-1 from pEK7 using Nco I restriction enzyme.	
pRGS49	*Psrsx-3::srsx-3::mKate2*	Visualization of GPCR SRSX-3 in the cilia of AWC^{OFF} neuron.	Obtained by Gibson cloning: PCR-amplified fragments *Psrsx-3::srsx-3* (org633/org634) and *mKate2::3'UTR unc-54* (org631/org632) were assembled with Spe I-linearized pCFJ910 plasmid [17].	org631 TCCGAGCTCATCAAG GAGAAC org632 CATTCGAAGATCTGC CCACTAGAAACAGTT ATGTTTGGTATATTG org633 AAGCTACGTAATACG

				ACTCATAATCGTTAA CTGTATTG org634 GTTCTCCTTGATGAG CTCGGATTGTTTGCT TGAATCCATCAC
pRGS48	*Pstr-1::eff-1*	Together with pEK12, AWC^{ON}-AWB fusion.	Obtained by Gibson cloning: PCR-amplified fragment *Pstr-1* (oEK28/oEK29) was assembled with Spe I/Kpn I-linearized pRGS8 plasmid.	oEK28 AAATGAAATAAGCTT GCATGCCAGTAAAAT GAATTGAGAGTG oEK29 AAACGGCGGTTCCAT GGTACTAGTCAAATG ATATGAAGTTTGTG
pRGS51	*Pstr-1::(empty)*	*Pstr-1* control.	Obtained by removing *eff-1* from pRGS48 using Nco I restriction enzyme.	
pEK12	*Pstr-2::eff-1*	Together with pRGS48, AWC^{ON}-AWB fusion.	Obtained by Gibson cloning: PCR-amplified fragment *Pstr-2* (oEK28/oEK29) was assembled with Sph I/Kpn I-linearized pRGS8 plasmid.	oEK AAATGAAATAAGCTT GCATGAGAGACAGG ATACAACTGATAATA oEK AAACGGCGGTTCCAT GGTACTTTTATGGAT CACGAGTATTC
pRGS52	*Pstr-2::(empty)*	*Pstr-2* control.	Obtained by removing *eff-1* from pEK12 using Nco I restriction enzyme.	
pRGS10	*Pstr-2::Kaede*	Expression of Kaede in AWC^{ON}.	Obtained by cloning PCR amplified *Pstr-2* into pRGS9 (pSM::*Kaede*) using Sph I and Bam HI restriction enzymes.	org397 ACATGCATGCAGAGA CAGGATACAACTGAT AATAC org398 CGCGGATCCTTTTAT GGATCACGAGTATT
pSC2	*Pmec-4::eff-1*	Together with pRGS17, PLN-PLM fusion.	[18]	
pRGS17	*Plad-2::eff-1*	Together with pSC2, PLN-PLM fusion.	Obtained by replacing *Pmec-4* with *Plad-2* (from *Plad-2::mCherry*) in pSC2 using Sph I and Sal I restriction enzymes.	
	Plad-2::mCherry	Expression of a cytoplasmic red fluorophore in PLN.	[15]	
pRGS12	*PF16F9.3::aff-1*	Together with pRGS6, AWC-AWB-AMsh fusion.	Obtained by replacing *Podr-1* with PCR-amplified *PF16F9.3* in pRGS6, using Hind III and Kpn I restriction enzymes.	org454 CCCAAGCTTCAAAAA GTGCGATAAGATCG org453 CGGGGTACCATTTTG TTTCTTACTGTCTTG

pKG18	*Pstr-1::mCherry::rab-3*	Expression of a red fluorophore tagged RAB-3.	Obtained by replacing *Pglr-3* in pAD5 (*Pglr-3::mCherry::rab-3*) with PCR amplified *Pstr-1* using Fse I and Asc I restriction enzymes.	FseI Pstr1 F2 TAAGCAGGCCGGCCG AGTGAGAAGAATGTC AC AscI Pstr1 R2 TGCTTAGGCGCGCCT AGTCAAATGATATGA AGTTTGTG

Supplementary Information References

1 Smurova, K. & Podbilewicz, B. Endocytosis regulates membrane localization and function of the fusogen EFF-1. *Small GTPases* **8**, 177-180, doi:10.1080/21541248.2016.1211399 (2017).

2 Shemer, G. *et al.* EFF-1 is sufficient to initiate and execute tissue-specific cell fusion in *C. elegans*. *Curr Biol* **14**, 1587-1591, doi:10.1016/j.cub.2004.07.059 (2004).

3 Troemel, E. R., Kimmel, B. E. & Bargmann, C. I. Reprogramming chemotaxis responses: sensory neurons define olfactory preferences in *C. elegans*. *Cell* **91**, 161-169 (1997).

4 Hart, A. C. in *WormBook* (ed WormBook The *C. elegans* Research Community) (2006).

5 Wes, P. D. & Bargmann, C. I. *C. elegans* odour discrimination requires asymmetric diversity in olfactory neurons. *Nature* **410**, 698-701, doi:10.1038/35070581 (2001).

6 Bargmann, C. I., Hartwieg, E. & Horvitz, H. R. Odorant-selective genes and neurons mediate olfaction in *C. elegans*. *Cell* **74**, 515-527 (1993).

7 Wang, W. *et al.* Off-response in ASH neurons evoked by CuSO4 requires the TRP channel OSM-9 in *Caenorhabditis elegans*. *Biochem Biophys Res Commun* **461**, 463-468, doi:10.1016/j.bbrc.2015.04.017 (2015).

8 Lesch, B. J., Gehrke, A. R., Bulyk, M. L. & Bargmann, C. I. Transcriptional regulation and stabilization of left-right neuronal identity in *C. elegans*. *Genes Dev* **23**, 345-358, doi:10.1101/gad.1763509 (2009).

9 Tursun, B., Patel, T., Kratsios, P. & Hobert, O. Direct conversion of *C. elegans* germ cells into specific neuron types. *Science* **331**, 304-308, doi:10.1126/science.1199082 (2011).

10 Zallen, J. A., Kirch, S. A. & Bargmann, C. I. Genes required for axon pathfinding and extension in the *C. elegans* nerve ring. *Development* **126**, 3679-3692 (1999).

11 Procko, C., Lu, Y. & Shaham, S. Glia delimit shape changes of sensory neuron receptive endings in *C. elegans*. *Development* **138**, 1371-1381, doi:10.1242/dev.058305 (2011).

12 Chang, C., Hsieh, Y. W., Lesch, B. J., Bargmann, C. I. & Chuang, C. F. Microtubule-based localization of a synaptic calcium-signaling complex is required for left-right neuronal asymmetry in *C. elegans*. *Development* **138**, 3509-3518, doi:10.1242/dev.069740 (2011).

13 Olivier-Mason, A. *et al.* Transmembrane protein OSTA-1 shapes sensory cilia morphology via regulation of intracellular membrane trafficking in *C. elegans*. *Development* **140**, 1560-1572, doi:10.1242/dev.086249 (2013).

14 Troemel, E. R., Sagasti, A. & Bargmann, C. I. Lateral signaling mediated by axon contact and calcium entry regulates asymmetric odorant receptor expression in *C. elegans*. *Cell* **99**, 387-398 (1999).

15 Neumann, B., Nguyen, K. C., Hall, D. H., Ben-Yakar, A. & Hilliard, M. A. Axonal regeneration proceeds through specific axonal fusion in transected *C. elegans* neurons. *Dev Dyn* **240**, 1365-1372, doi:10.1002/dvdy.22606 (2011).

16 Leinwand, S. G. & Chalasani, S. H. Neuropeptide signaling remodels chemosensory circuit composition in *Caenorhabditis elegans*. *Nat Neurosci* **16**, 1461-1467, doi:10.1038/nn.3511 (2013).

17 Frokjaer-Jensen, C. *et al.* Random and targeted transgene insertion in *Caenorhabditis elegans* using a modified Mos1 transposon. *Nat Methods* **11**, 529-534, doi:10.1038/nmeth.2889 (2014).

18 Neumann, B. *et al.* EFF-1-mediated regenerative axonal fusion requires components of the apoptotic pathway. *Nature* **517**, 219-222, doi:10.1038/nature14102 (2015).